ELSEVIER

Biochemical Pharmacology 62 (2001) 297–306

Biochemical Pharmacology

Hepatic distribution of a phosphorothioate oligodeoxynucleotide within rodents following intravenous administration

Mark J. Graham*, Stanley T. Crooke, Kristina M. Lemonidis, Hans J. Gaus, Michael V. Templin, Rosanne M. Crooke

ISIS Pharmaceuticals, Inc., Carlsbad Research Center, 1896 Rutherford Rd., Carlsbad, CA 92008, USA

Received 11 July 2000; accepted 7 November 2000

Abstract

The pharmacokinetics of ISIS 1082, a 21-base heterosequence phosphorothioate oligodeoxynucleotide, were characterized within rodent whole liver, and cellular and subcellular compartments. Cross-species comparisons were performed using Sprague–Dawley rat and CD-1 mouse strains. Although whole liver oligonucleotide deposition and the proportion of drug found within parenchymal and nonparenchymal cells were similar between the two rodent species as a function of both time and dose, dramatic differences in subcellular pharmacokinetics were observed. Specifically, within murine hepatocyte nuclei, drug was observed at the 10 mg/kg dose, whereas in the rat nuclear-associated levels required the administration of 25 mg/kg. Under all experimental regimens, murine hepatic nuclear-associated drug concentrations were at least 2-fold higher than those found in rat liver cells. More detailed metabolic analysis was also performed using high performance liquid chromatography/electrospray-mass spectrometry (HPLC/ES-MS) and demonstrated that although the extent of metabolism was similar for rat and mouse, the pattern of n-1 metabolites varied as a function of both species and cell type. While rat and mouse hepatocytes and rat nonparenchymal cellular metabolites were predominantly products of 3′-exonuclease degradation, mouse nonparenchymal cells contained a majority of n-1 metabolites produced by 5′-exonucleolytic activity. Based upon these data, it would appear that subcellular oligonucleotide disposition and metabolism among rodent species are more divergent than whole organ pharmacokinetics might predict.

Keywords: Antisense; Oligonucleotide; Pharmacokinetics; Rodent; Capillary gel electrophoresis; Hepatic

1. Introduction

Antisense oligonucleotides represent a new class of therapeutic agents that are widely used, both *in vitro* and *in vivo*, to determine the roles of gene products in a variety of disease states [1,2]. The pharmacokinetics of phosphorothioate oligodeoxynucleotides have been characterized in multiple species and, in fact, these compounds have been administered to several thousands of patients. They are rapidly and efficiently absorbed from all parenteral sites studied [1,3–5], and display dose-dependent pharmacokinetics for the following reasons: (a) at high doses they saturate albumin binding sites; (b) as doses are increased, primary tissues of distribution are saturated and other tissues accumulate greater amounts of drug; and (c) at higher doses, exo- and endonucleases are inhibited, lengthening elimination half-lives [1,2,6,7]. Additionally, there is no evidence that their pharmacokinetic properties are affected by the presence or absence of their target RNAs in tissues. This is not surprising since most target RNAs are present at only 1–10 copies of RNA per cell [8].

A number of recent *in vivo* experiments have begun to address cellular distribution and intracellular localization of phosphorothioate oligodeoxynucleotides in a variety of organs and tumor isolates following systemic administration [6,9–11]. These studies indicated that the majority of cellular uptake occurred within renal proximal convoluted tubular cells, skin fibroblasts, and dendritic cells, and within hepatocytes, Kupffer cells, and endothelial cells of the liver.

* Corresponding author. Tel.: +1-760-603-2344; fax: +1-760-931-0209.

E-mail address: mgraham@isisph.com (M.J. Graham).

[1]Johnston J, ISIS Pharmaceuticals, personal communication. Cited with permission.

Abbreviations: HSV, herpes simplex virus; CGE, capillary gel electrophoresis; and HPLC/ES-MS, high performance liquid chromatography/electrospray-mass spectrometry.

0006-2952/01/$ – see front matter
PII: S0006-2952(01)00669-4

While the previously cited studies relied on indirect detection, radiolabeling, or fluorescent oligonucleotide conjugates, we directly measured subcellular concentrations and the metabolic stability of a 21-mer phosphorothioate oligodeoxynucleotide (ISIS 1082) in rat liver following intravenous administration, utilizing previously described cellular isolation, fractionation, and analytical techniques [12–15]. Our data showed that rat nonparenchymal cells retained approximately 80% of the oligonucleotide present within all hepatic cell types. This level was equally distributed between Kupffer and endothelial cells, while the remaining 20% was localized within hepatocytes. Differences in the dose at which saturation was observed varied as a function of cell type. Specifically, nonparenchymal cells appeared to be saturated after intravenous doses in excess of 25 mg/kg, whereas in hepatocytes no saturation was evident even at the highest dose administered (50 mg/kg). We also performed subcellular fractionation to derive nuclear, cytosolic, and membrane distribution patterns as a function of cell type. Our studies demonstrated that doses above 10 mg/kg were required to observe nuclear-associated oligonucleotide within rat hepatocytes, whereas nonparenchymal cell nuclei contained oligonucleotide even at the lowest dose administered (5 mg/kg).

Because many current pharmacological studies with antisense drugs are performed in mice rather than in rats [16–19], we believed it was important to determine the similarities and differences in pharmacokinetic parameters between rodent species. The findings reported in this study reveal that although general distribution trends were conserved as a function of whole organ and cell type, the level of phosphorothioate oligodeoxynucleotide internalized within subcellular compartments was highly divergent.

In this study, we employed ISIS 1082, a 21-mer phosphorothioate oligodeoxynucleotide that is complementary to a mRNA sequence in the human HSV type 2 gene. Computer analysis revealed no significant homology to sequences present in mouse or rat liver. As ISIS 1082 has been administered extensively in both rats and monkeys, it is a useful drug to compare suborgan pharmacokinetics in the two rodent species.

2. Materials and methods

2.1. Oligonucleotide synthesis

ISIS 1082 (GCCGAGGTCCATGTCGTACGC), a uniform 21-base phosphorothioate oligodeoxynucleotide, was synthesized at ISIS Pharmaceuticals on a Milligen 8800 DNA synthesizer by the phosphoramidite method. The thiation reagent was synthesized as described previously [20]. The oligomer was purified using reversed-phase HPLC and determined to be greater than 85% full length by CGE. ISIS 1082 is targeted to a sequence in HSV type 2. A BLAST search revealed no mouse gene sequences containing significant homology.

2.2. Animals

Male Sprague–Dawley rats (200–300 g) were obtained from Harlan Sprague–Dawley. The mouse strain used for comparison was CD-1 (Charles River Laboratories) with animal weights ranging from 25 to 35 g. The animals were housed in polycarbonate cages with food and water available *ad lib.* Care was in compliance with guidelines of the Institutional Animal Care and Use Committee of ISIS Pharmacueticals. Doses of 5, 10, 25, 50, or 100 mg/kg were administered by intravenous injection (tail vein), and animals were killed after 24 hr. Time–course experiments were conducted using a 10 mg/kg dose.

2.3. Liver perfusion

The liver was perfused, with minor modification, as described previously [11,20,21]. Rats were anesthetized with an intraperitoneal injection of sodium pentobarbital, while for mouse studies tribromoethanol (Avertin®) was used. Following collagenase treatment, the livers were removed and placed in 100 mL of ice-cold 1X PBS. After gentle shaking, the suspension was poured through sterile 260 μm nylon mesh (Tetko).

2.4. Purification of parenchymal and nonparenchymal cells

Hepatocytes and Kupffer and endothelial cells were isolated from whole liver as described previously [12,21–23]. Hepatocytes were isolated from the liver perfusate as referenced above, by centrifugation at 50 *g* for 5 min at 4° in a Beckman tabletop centrifuge. Nonparenchymal cells were further separated into endothelial and Kupffer cell populations by brief adherence to plastic at 37° followed by trypsinization and cell scraping to take advantage of the differential adherence characteristics of the two cell types [12,24]. Cellular enrichment, as assessed using immunohistochemical markers described previously [12], was approximately 90% for hepatocytes and 80% for Kupffer and endothelial cell isolates.

2.5. Subcellular fractionation

The fractionation procedure used to isolate nuclear, membrane, and cytosolic constituents was performed as described previously, with minor modification [12,13]. Cell lysis was accomplished using an isotonic buffer consisting of 0.5% NP-40, 10 mM Tris–Cl (pH 7.4), 140 mM KCl, 5 mM $MgCl_2$, and 1 mM dithiothreitol [25]. Following lysis, nuclei were maintained at 4° and isolated by centrifugation for 5 min at 1310 *g*. Membrane constituents were separated from cytosol by transfer to thick-walled polycarbonate tubes

and centrifugation (200,000 *g*) for 30 min at 4° in a Beckman TLA 100.2 fixed angle rotor using a Beckman TL-100 benchtop ultracentrifuge. Following centrifugation, the supernatant represented purified cytosol, while the pellet contained plasma membrane and various subcellular organelles including endosomes and lysosomes. Previous control experiments using this technique indicated minimal cross-contamination between the various isolated fractions [13].

2.6. Cellular digestion and organic extraction for CGE analysis

Whole cells and cellular fractions were digested using proteinase K extraction solution, as described previously [12,13]. Samples were incubated for 2 hr at 55° to digest proteins after the addition of 30 pmol of an internal standard (polyT 27-mer phosphorothioate oligodeoxynucleotide). After digestion, 200 μL of 30% ammonium hydroxide was added to each sample prior to organic extraction using 1 mL of phenol:isoamyl alcohol:chloroform (24:1:24, by vol.) [12,14].

2.7. Solid phase extraction and CGE analysis

To purify samples sufficiently for CGE, two solid phase extraction columns were required [14]. Briefly, removal of residual contaminants was accomplished using a strong anion exchange solid phase extraction column (J & W Scientific) followed by desalting using a reversed-phase solid phase extraction column (Isolute endcapped C18). A final desalting step was employed prior to CGE analysis to further reduce the amount of competitive anions that would be loaded during electrokinetic injections. Samples were placed on 0.025 μm dialysis membranes (Millipore) and floated over 60-mm culture dishes containing 10 mL of 18.3 MΩ-cm dH_2O for 30 min prior to analysis.

Following dialysis, samples were placed into microvials and analyzed using a Beckman PA/CE 5010 capillary electrophoresis system with UV-detection at A_{260} nm as described previously [12]. Samples were electrokinetically applied using 5–10 kV for 5–10 sec, while separations were achieved operating at 20 kV constant voltage in approximately 5 min at 50°. Samples were injected and quantified within the linear range of the detector, which spanned approximately 0.01 to 0.001 measured absorbance units.

Comparison of the absorbance and migration time of the internal standard (T27) with the absorbance and migration time of oligonucleotide metabolites allowed for sample quantification. All whole cell and fractionation results are expressed as the number of molecules detected per cell.

2.8. HPLC/ES-MS analysis

Oligonucleotide samples were desalted prior to analysis using a 2 $\times$ 150 mm HPLC Luna C18 column. Buffer A contained 2 mM tripentylammonium actetate in 30% acetonitrile. Buffer B consisted of 2 mM tripentylammonium acetate in 70% acetonitrile. A linear gradient from 100% A to 199% B was achieved after 25 min with a flow rate of 200 μL/min. Mass spectra were acquired using Hewlett-Packard MSD 1100 or Finnigan LCQ instruments. The -4 charge state was used for identification and quantification of ISIS 1082 and metabolites present within cellular isolates.

3. Results

3.1. Rodent liver distribution as a function of time

For comparison of whole organ pharmacokinetics in Sprague–Dawley rats versus CD-1 mice, animals were dosed by i.v. bolus injection and killed at 1, 4, 8, and 24 hr following a drug dose of 10 mg/kg. The concentration of intact drug and metabolites as a function of time was determined by CGE analysis using 100 mg of whole liver tissue (Table 1). After 1 hr, total drug levels were approximately 4 μM for both species, with maximum liver concentrations observed by 8 hr. In general, CD-1 mice displayed slightly higher drug levels than Sprague–Dawley rats at all the time points measured, with the greatest difference seen at 8 hr after dosing (7 μM for mouse and 5 μM for the rat). At 24 hr, the concentration of drug had decreased in both mice and rats to approximately 4 and 3 μM, respectively.

3.2. Effect of dose on distribution to rodent liver

ISIS 1082 was administered by i.v. bolus at 5, 25, 50, and 100 mg/kg, and tissue was collected 24 hr after dosing (Table 2). In both species, the level of ISIS 1082 increased in a dose-dependent manner from approximately 4 to 13 μM at the 5 to 50 mg/kg dose levels, respectively. At doses above 50 mg/kg, both rat and mouse livers appeared to be saturated, with no significant increase in drug accumulation evident. At doses above 5 mg/kg, mice displayed greater average drug concentrations than those observed in rats. These differences were statistically significant at doses of 25 and 100 mg/kg with *P* values of 0.01 and 0.03, respectively.

3.3. Suborgan distribution of ISIS 1082

3.3.1. Kinetics

At specified intervals following 10 mg/kg i.v. administration, parenchymal and nonparenchymal cells were isolated to determine species-specific oligonucleotide distribution patterns (Fig. 1). At all time points and in both rodent species, Kupffer and endothelial cells contained a majority of the cell-associated drug. Nonparenchymal cells had approximately twice the amount of ISIS 1082 that accumulated in hepatocytes. Within rat hepatocytes, the proportion of ISIS 1082 and metabolites was maximal after 1 hr and

Table 1
Effect of time on the level of ISIS 1082 and metabolites within 100 mg of homogenized whole Sprague–Dawley rat or CD-1 mouse liver after 10 mg/kg i.v. administration

Time after dose (hr)	Drug level (μM)	
	Sprague-Dawley rat	CD-1 mouse
1	4.2 ± 0.6	4.4 ± 0.4
4	3.8 ± 0.1	5.8 ± 0.5
8	4.7 ± 0.4	7.0 ± 0.6
24	2.7 ± 0.1	3.8 ± 0.1

The drug level is expressed in a micromolar amount of intact drug and metabolites detected, and each point represents the mean ± SEM of three animals.

decreased in a linear fashion over 24 hr. In contrast, peak drug levels in mouse hepatocytes were achieved after 4 hr and decreased thereafter. Within Kupffer cells the proportion of drug remained relatively constant over 24 hr. The greatest differences were observed when endothelial cells were compared. Specifically, in rat endothelial cells C_{max} occurred after 4 hr and declined thereafter, whereas within mouse endothelial cells the proportion of ISIS 1082 and metabolites continued to increase over 24 hr.

3.3.2. Dose response

As the dose administered to animals was increased from 5 to 50 mg/kg, the proportion of ISIS 1082 and metabolites detected after 24 hr increased in a dose-dependent manner within both rat and mouse hepatocytes (Fig. 2). In nonparenchymal cells, saturation was evident at doses between 5 and 10 mg/kg depending on the cell type, with no saturation apparent for hepatocytes in either species.

3.4. Subcellular localization

3.4.1. Kinetics

Within rat hepatocytes no nuclear-associated drug was detected at any time, whereas in murine hepatocyte nuclei ISIS 1082 and metabolites were observed over the entire time course (Fig. 3A). The highest nuclear, cytosolic, and membrane drug levels were attained 4 hr post dose in mice,

Table 2
Effect of dose on the accumulation of ISIS 1082 and metabolites in 100 mg of homogenized whole Sprague–Dawley rat or CD-1 mouse liver after an i.v. bolus of 5, 25, 50 and 100 mg/kg, respectively

Dose (mg/kg)	Drug level (μM)	
	Sprague–Dawley rat	CD-1 mouse
5	4.0 ± 0.9	3.4 ± 0.4
25	5.9 ± 0.5	9.2 ± 0.7
50	12 ± 2.0	14 ± 1.5
100	13 ± 0.4	18 ± 3.5

The drug level is expressed in a micromolar amount of intact drug and metabolites detected, and each point represents the mean ± SEM of three animals.

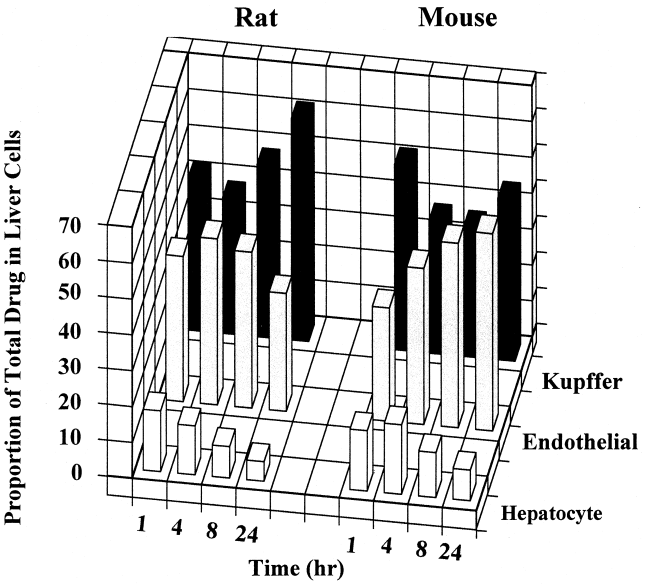

Fig. 1. Effect of time on the proportion of ISIS 1082 and metabolites found in whole rat and mouse liver cells after a 10 mg/kg i.v. bolus dose. Sprague–Dawley rat hepatic cells are shown on the left and CD-1 mouse liver cells on the right. Values for each bar represent the mean of intact drug and metabolites and are expressed as a percentage of the total liver cell dose. The identity of each cell type is displayed on the lower right side of the plot. Replicates are as follows: hepatocytes (N = 9, SEM ± 10%), Kupffer cells (N = 3, SEM ± 20%), and endothelial cells (N = 4, SEM ± 12%).

whereas in the rat peak oligonucleotide levels in the membrane and cytosolic fractions were observed after 8 hr.

Significant differences in subcellular pharmacokinetics were also evident in Kupffer cells (Fig. 3B). Mouse Kupffer cytosol and membrane appeared to accumulate drug more readily than these same tissues in the rat, and peak concentrations of drug were greater in mouse Kupffer cell membranes. Similar kinetics were observed within endothelial cellular fractions (Fig. 3C). Regardless of the apparent differences in the rate of cytosolic and membrane drug clearance, by 24 hr, murine endothelial and Kupffer cell nuclear-associated drug levels remained 3- and 8-fold greater, respectively, than those measured in rat nonparenchymal cell nuclei.

3.4.2. Dose response

In both species, dose-dependent increases in ISIS 1082 and metabolites were detected, with pronounced differences observed in hepatocyte subcellular fractions (Fig. 4A). At the 5 mg/kg dose level, nuclear-associated drug was not evident in either rat or mouse hepatocytes. However, at 10 mg/kg, murine hepatocytes had readily detectable nuclear-associated drug. In contrast, in order to detect ISIS 1082 and metabolites in the nucleus of rat hepatocytes, a minimum dose of 25 mg/kg was required. Within both species and all three cellular fractions, there was no evidence of saturation up to the 50 mg/kg dosage. Consistent with our previous observations, murine hepatocyte cellular fractions exhibited

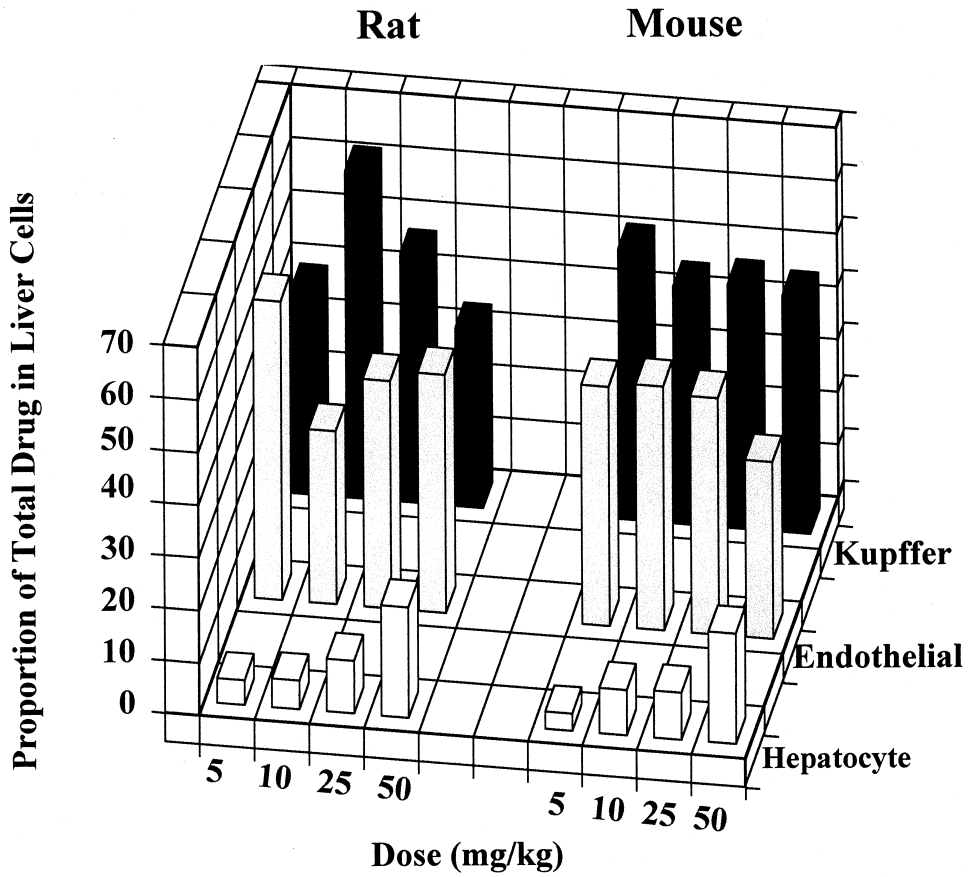

Fig. 2. Effect of dose on the proportion of ISIS 1082 and metabolites in whole rat and mouse liver cells after an i.v. bolus of 5, 10, 25, or 50 mg/kg, respectively. Sprague–Dawley rat hepatic cells are shown on the left and CD-1 mouse liver cells on the right. Values for each bar represent the mean of intact drug and metabolites and are expressed as a percentage of the total liver cell dose. The identity of each cell type is shown on the lower right side of the plot. Replicates are as follows: hepatocytes (N = 9, SEM ± 8%), Kupffer cells (N = 3, SEM ± 15%), and endothelial cells (N = 4, SEM ± 10%).

2-fold higher drug concentrations relative to rat hepatocytes, at doses above 5 mg/kg, with the greatest differences found in nuclear and membrane fractions.

Data derived from nonparenchymal cell fractions demonstrated even greater differences in intracellular distribution patterns. In rat Kupffer cell isolates, the majority of ISIS 1082 and metabolites were found in the cytosolic fraction, with saturation at doses higher than 10 mg/kg (Fig. 4B). In contrast, murine Kupffer cell fractions contained similar amounts of drug, with saturation occurring above 25 mg/kg. As seen before, the murine nuclear and membrane fractions contained, on average, substantially higher drug levels measured relative to those within rat Kupffer cell fractions, respectively. Similar differences were observed between rat and mouse endothelial subcellular fractions (Fig. 4C).

3.5. Metabolism

A major advantage of CGE analysis is that it provides a means for directly measuring oligonucleotide concentrations while simultaneously facilitating detailed metabolic assessment. In an earlier publication [12], we observed that a majority of ISIS 1082 metabolism occurred within the first hour after systemic administration of drug. No significant differences in metabolism were evident when whole organ and cellular and subcellular fractions were compared. At 24 hr following a 10 mg/kg i.v. bolus dose, there was only a 10% reduction in percent full-length oligonucleotide relative to the level observed after 1 hr, suggesting that a majority of the hepatic metabolites were produced extracellularly. Results from dose–response experiments suggested

Table 3
Pattern of ISIS 1082 n-1 metabolites generated as a function of rodent liver cell type 24 hr after 100 mg/kg i.v. administration

Liver cell type	3′/(5′ + 3′) ISIS 1082 n-1 metabolites	
	Sprague-Dawley rat	CD-1 mouse
Hepatocyte	74 ± 2.2	78 ± 6.6
Kupffer	72 ± 3.0	22 ± 2.9
Endothelial	75 ± 1.9	42 ± 0.9

The mean ratios of 3′/(5′ + 3′) n-1 degradation species are shown for hepatocytes (N = 9), Kupffer cells (N = 3), and endothelial cells (N = 3). The SEM is indicated for each set of replicates.

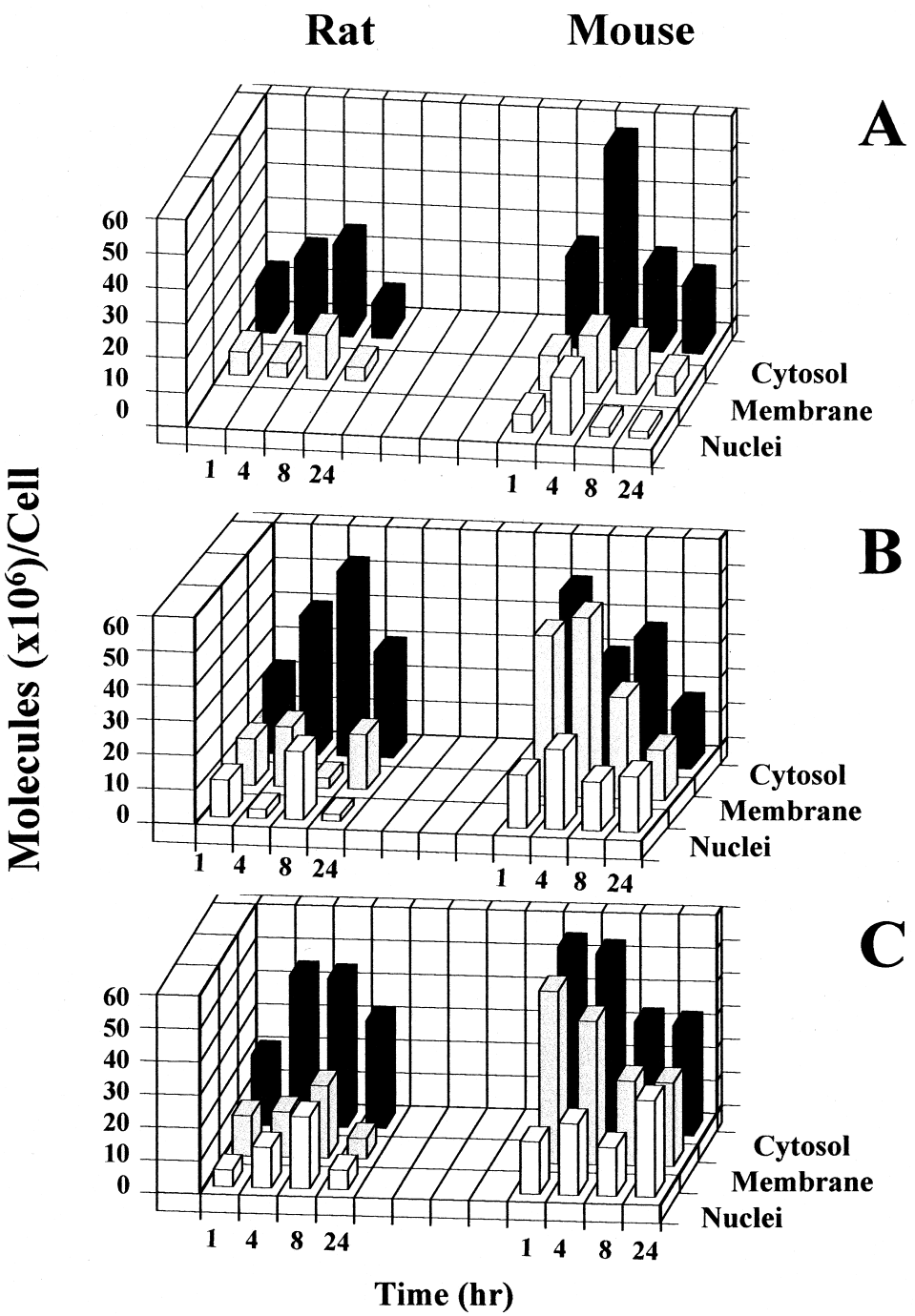

Fig. 3. Subcellular localization of ISIS 1082 and metabolites over a 24-hr period within rodent hepatocytes (panel A), Kupffer cells (panel B), and endothelial cells (panel C). Sprague–Dawley rat liver cells are shown on the left and CD-1 mouse cells on the right. Each bar represents the mean of intact drug and metabolites expressed in molecules (x 10^6)/cell. The identity of each nuclear cytosolic and membrane fraction is indicated on the lower right side of the plot. Each bar represents the average of 9 replicate isolations for hepatocytes (SEM ± 5%), 3 replicates for Kupffer cells (SEM ± 18%), and 4 replicates for endothelial cells (SEM ± 13%).

a moderate decrease in the rate of metabolism of ISIS 1082 in rat whole liver as the dosage was increased.

The metabolic trends within mouse whole liver, hepatic cells, and subcellular fractions were consistent with those first observed in the rat (data not shown) [12]. Specifically, 24 hr after dosing, intact ISIS 1082 represented 35–40% of the total oligonucleotide present in both rodent species. These results suggest that the relative abundance and localization of the nucleases, both endo and exo, responsible for phosphorothioate oligodeoxynucleotide metabolism *in vivo*, are similar within rodent species.

Although CGE is capable of measuring metabolism of oligonucleotides with single-base resolution, it cannot resolve whether metabolites are the product of 5′ or 3′ trun-

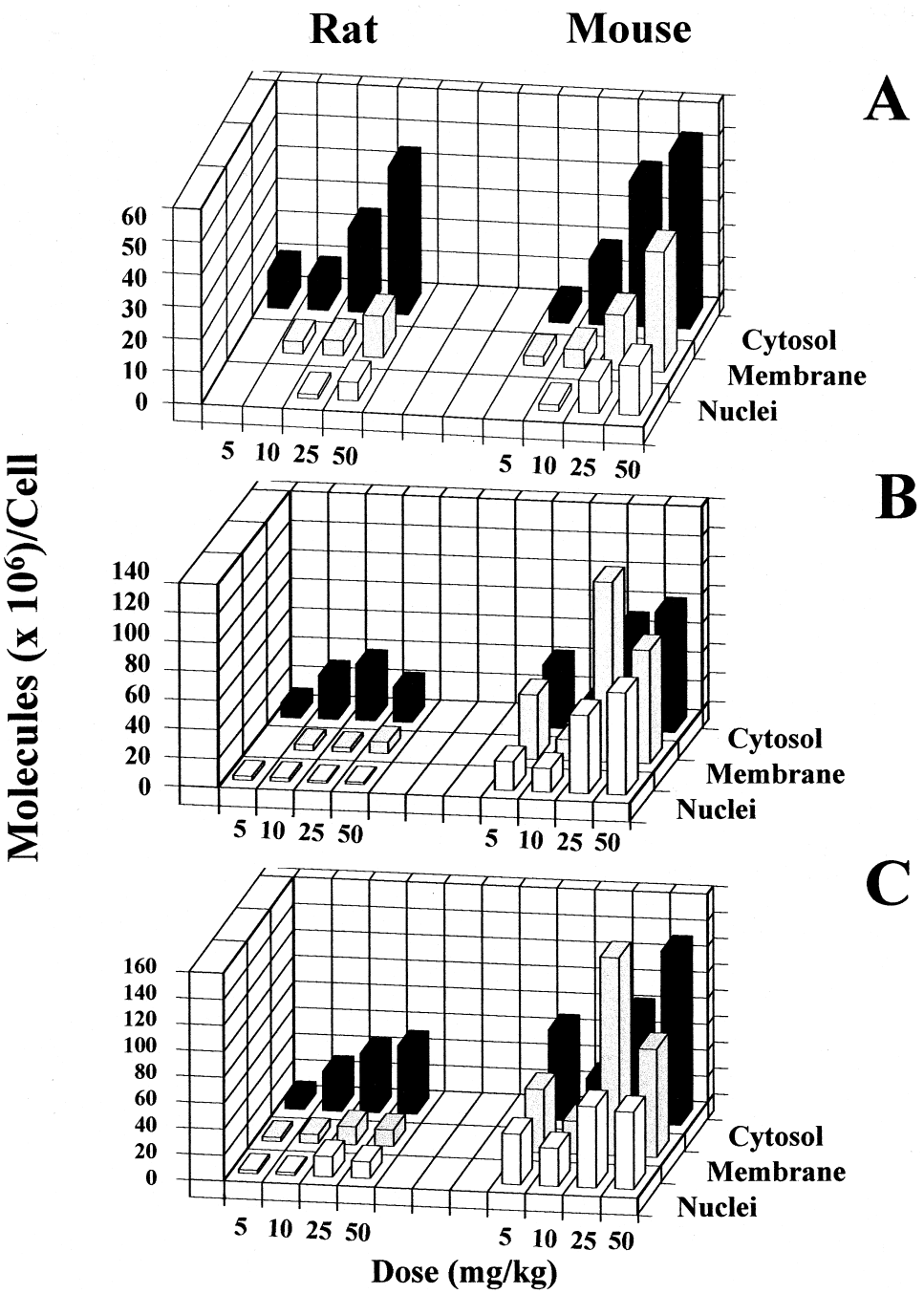

Fig. 4. Subcellular distribution of ISIS 1082 and metabolites 24 hr after 5, 10, 25, and 50 mg/kg i.v. within rodent hepatocytes (panel A), Kupffer cells (panel B), and endothelial cells (panel C). Sprague–Dawley rat liver cells are shown on the left and CD-1 mouse hepatocyte values on the right. Each bar represents the mean of intact drug and metabolites expressed in molecules (x 10^6)/cell. The identity of each nuclear, cytosolic, and membrane fraction is indicated on the lower right side of the plot. Each bar represents the average of 9 hepatocyte isolations (SEM ± 8%), 3 Kupffer replicates (SEM ± 23%), and 4 endothelial replicates (SEM ± 20%). Note that at the 5 mg/kg dosage, no drug could be measured in either rat or mouse hepatocyte nuclei. This was also the case for rat isolates at the 10 mg/kg dose level.

cation of the molecule. For this reason, we performed HPLC/ES-MS analysis of rodent liver cell isolates to definitively identify degradation pathways. Using previously described techniques [26,27], the results derived from rodent liver cells 24 hr after i.v. administration of 100 mg/kg of ISIS 1082 are expressed as the ratio of 3′/(5′ + 3′) n-1 metabolites of ISIS 1082 (Table 3). We chose to analyze this dose group because it represented the highest drug level attained within hepatocytes and, thus, the best signal-to-noise ratio for comparing metabolic profiles among the various liver cell types. While both rat and mouse hepatocytes contained roughly equivalent metabolic ratios (i.e. 70–75% n-1 species due to 3′-exonuclease activity), substantial differences were observed in nonparenchymal cells

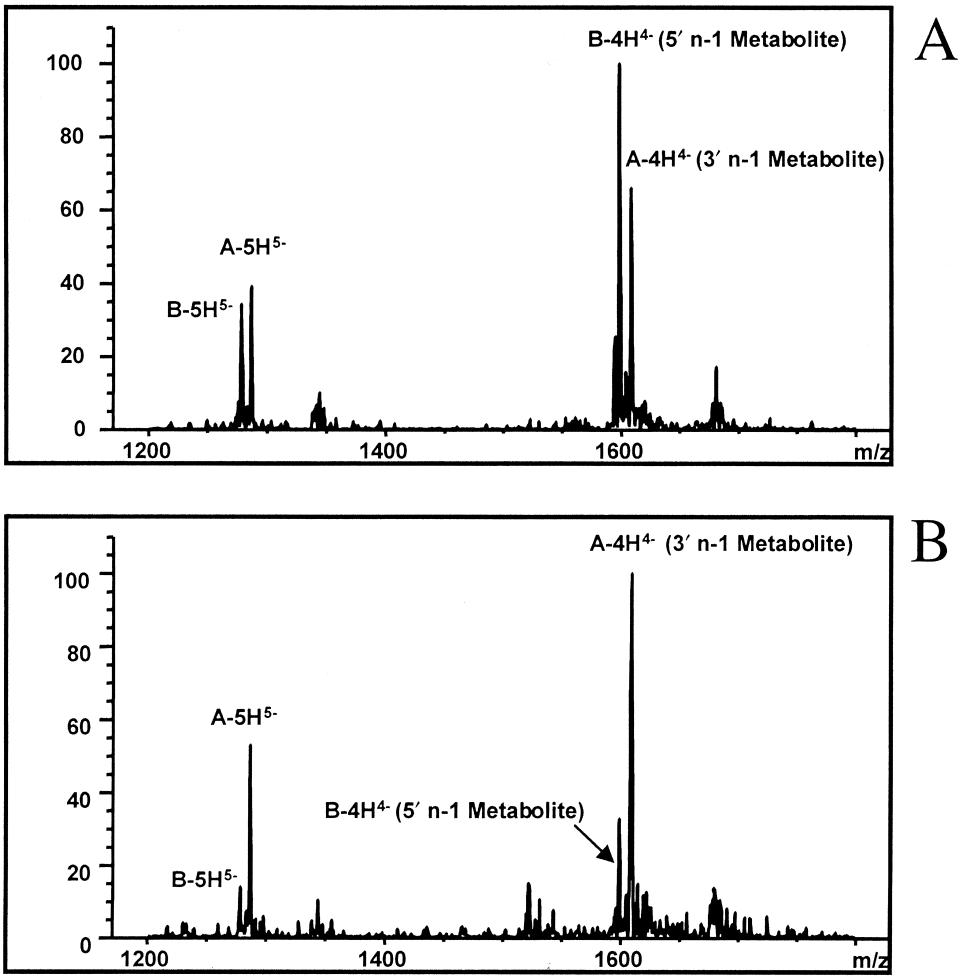

Fig. 5. HPLC/ES-MS histograms of ISIS 1082 n-1 metabolites generated from mouse (panel A) and rat (panel B) endothelial cells 24 hr after 100 mg/kg intravenous administration. Both the –4 and –5 charge states of the respective 3′ (A) and 5′ (B) n-1 degradation products are indicated. Note that the 5′ n-1 metabolite (B-$4H^{4-}$) is the major species in the mouse endothelial cells, whereas in rat endothelial cells the 3′ n-1 metabolite (A-$4H^{4-}$) is more predominant.

(Fig. 5), where mouse cell degradation products were predominantly the result of 5′-exonucleolytic cleavage.

4. Discussion

Our laboratory recently published the first complete analysis of phosphorothioate oligodeoxynucleotide disposition and metabolism within the whole rat liver, hepatic cell types, and subcellular compartments [12]. Since an ever-increasing number of antisense pharmacological studies are performed in a variety of mouse models [16,19,28,29], our principal goal for the current study was to determine whether the hepatic distribution and metabolism in CD-1 mice are comparable to those in Sprague–Dawley rats [12].

Data from *in vivo* experiments in mouse, rat, and monkey after systemic administration of phosphorothioate oligodeoxynucleotides suggest that gross tissue distribution and other pharmacokinetic parameters are independent of route of administration, sequence, and, most importantly, species [5]. In this study, when whole liver distribution was compared after systemic administration of ISIS 1082, subtle, but detectable, differences between the two species became evident. Kinetic experiments performed over a 24-hr period following a 10 mg/kg i.v. bolus dose indicated that slightly higher concentrations of ISIS 1082 and metabolites were observed in mice (1.5-fold) relative to rats. These trends were also observed when dose–response studies were conducted.

Experiments using purified rodent whole parenchymal and nonparenchymal cells demonstrated many similarities, but also several important differences. In both rat and mouse, nonparenchymal cells accumulated significantly more drug than their corresponding hepatocytes. However, while the overall proportion and rate of clearance of ISIS 1082 and metabolites distributed within these various cells were similar, the time at which C_{max} occurred varied. For example, in murine hepatocytes, peak oligonucleotide levels occurred at 4 hr versus 8 hr for rat hepatocytes. Consistent with the whole organ observations of greater oligonucleo-

tide accumulation in mouse, absolute drug levels were 2- to 8-fold higher in murine versus rat hepatic cellular fractions under all conditions.

The most significant species-specific variations in pharmacokinetics were noted when the subcellular localization of ISIS 1082 was compared. These differences primarily related to: (a) the amount of compound present in hepatocyte and nonparenchymal cell nuclear and membrane fractions, and (b) the rate of clearance in all subcellular compartments. At lower doses of drug (5–10 mg/kg), no detectable oligonucleotide was observed in rat hepatocyte nuclei over a 24-hr period. In contrast, in mouse nuclear fractions, ISIS 1082 and metabolites were readily detected after a 10 mg/kg dose. Membranes in mice also contained higher amounts of drug compared with those in rats, ranging from 1.5- to 3-fold in hepatocytes, to 2- to 10-fold greater levels, on average, in Kupffer and endothelial cell isolates. Furthermore, mice eliminated drug faster and to a greater extent than rats (Fig. 3). Based upon studies comparing the tissue distribution of phosphorothioate oligodeoxynucleotide among multiple species, mice clear the oligonucleotide 2- to 3-fold faster from target tissue, including liver, than rats, monkeys, and humans and, therefore, would be less likely to accumulate drug compared with these species [5].

The overall extent of metabolism of ISIS 1082 in whole liver, hepatic cells, and subcellular fractions was similar, so that by 24 hr, the percentage of intact drug was 35–40% in both species. Also consistent between species was the rapid and extensive nucleolytic degradation of oligonucleotide in serum within the first hour after dosing.

However, HPLC/ES-MS analyses demonstrated that 3′-exonucleases are responsible for the majority (70–75%) of oligonucleotide degradation in rat hepatocytes, Kupffer cells, and endothelial cells. This predominance of 3′-exonuclease activity was also observed in murine hepatocytes, but not in mouse nonparenchymal cells where, in contrast, the majority of metabolites resulted from 5′-nucleotide elimination. These results demonstrated that, although the extent of metabolism is similar, there are significant interspecies differences involving the importance of 3′- versus 5′-exonucleases in the metabolism of ISIS 1082. The mechanisms responsible for the differences in suborgan distribution and metabolism are unknown. However, this study identifies for the first time such differences and lays the physiological foundation for determining the specific mechanisms of distribution and metabolism that are responsible for such species-specific variation.

In summary, although whole organ distribution of phosphorothioate oligodeoxynucleotides appears to be conserved in rodents, our experiments suggest that there are significant differences between mouse and rat on the suborgan and subcellular levels. The observation that there are pharmacokinetic differences between Sprague–Dawley rats and CD-1 mice is not without precedent. Other laboratories have also observed major differences in metabolism, $V_{max,}$ and the rate of elimination in those two species following administration of a variety of compounds, including methanol [30] and ethylene glycol [31]. In addition, when other strains of mice and rats were compared, variations in the rate of drug clearance, carcinogenicity, and metabolism have also been reported by others [32–35]. Our studies are unique, however, because we have quantified inter-species differences in disposition, clearance, and nuclease activities responsible for the metabolism of phosphorothioate oligodeoxynucleotides within hepatic cells and subcellular compartments.

The pharmacokinetic differences described above, most importantly, may help explain pharmacological results obtained in various studies. Based on *in vitro* experiments that have demonstrated that nuclear accumulation of phosphorothioate oligodeoxynucleotides was required for target mRNA inhibition [36], greater efficacy should be expected in mice due to significantly greater nuclear-associated drug concentrations. In fact, oligonucleotides designed to inhibit rodent C-*raf in vivo* consistently display greater antisense potency in mice compared with rats [1].

We also believe that distribution and metabolism of phosphorothioate oligonucleotides within the liver vary somewhat more substantially between species than might be predicted from previous whole organ pharmacokinetic studies. This may serve to explain some of the differences observed in the pharmacological activity among species. In addition, as only liver has been characterized in such detail thus far, it is possible that differences in pharmacokinetics are present within other organs as well. Importantly, while these studies with antisense drugs represent some of the first efforts to examine suborgan pharmacokinetics, other drug classes may display similar characteristics. Clearly, these types of studies have broad applicability for pharmaceutical research.

Acknowledgments

The authors wish to thank Drs. Janet Leeds and Len Cummins for their critical review and constructive comments with regard to this manuscript.

References

[1] Crooke ST. Basic principles of antisense therapeutics. In: Crooke ST, editor. Handbook of experimental pharmacology, antisense research and application. Berlin: Springer, 1998. p. 1–50.
[2] Crooke ST. Progress in antisense therapeutics: the end of the beginning. In: Abelson JN, Simon MI, editors. Antisense techniques. New York: Academic Press, 1999. p. 3–45.
[3] Cossum PA, Truong L, Owens SR, Markham PM, Shea JP, Crooke ST. Pharmacokinetics of a ^{14}C-labeled phosphorothioate oligonucleotide, ISIS 2105, after intradermal administration to rats. J Pharmacol Exp Ther 1994;269:89–94.
[4] Geary RS, Leeds JM, Fitchett J, Burckin T, Truong L, Spainhour C, Creek M, Levin AA. Pharmacokinetics and metabolism in mice of a

phosphorothioate oligonucleotide antisense inhibitor of C-*raf*-1 kinase expression. Drug Metab Dispos 1997;25:1272–81.
[5] Geary RS, Leeds JM, Henry SP, Monteith DK, Levin AA. Antisense oligonucleotide inhibitors for the treatment of cancer: 1. Pharmacokinetic properties of phosphorothioate oligodeoxynucleotides. Anticancer Drug Des 1997;12:383–93.
[6] Rifai A, Brysch W, Fadden K, Clark J, Schlingensiepen K. Clearance kinetics, biodistribution and organ saturability of phosphorothioate oligodeoxynucleotides in mice. Am J Pathol 1996;149:717–25.
[7] Nicklin PL, Craig SJ, Phillips JA. Pharmacokinetic properties of phosphorothioates in animals—absorption, distribution, metabolism and eliminination. In: Crooke ST, editor. Handbook of experimental pharmacology, antisense research and application. Berlin: Springer, 1998. p. 141–68.
[8] Miraglia L, Watt AT, Graham MJ, Crooke ST. Variations in mRNA content have no effect on the potency of antisense oligonucleotides. Antisense Nucleic Acid Drug Dev, in press.
[9] Zhao Q, Zhou R, Temsamani J, Zhang Z, Roskey A, Agrawal S. Cellular distribution of phosphorothioate oligonucleotide following intravenous administration in mice. Antisense Nucleic Acid Drug Dev 1998;8:451–8.
[10] Butler M, Stecker K, Bennett FL. Cellular distribution of phosphorothioate oligodeoxynucleotides in normal rodent tissues. Lab Invest 1997;77:379–88.
[11] Plenat F, Klein-Monohoven N, Marie B, Vignaud J, Duprez A. Cell and tissue distribution of synthetic oligonucleotides in healthy and tumor-bearing nude mice. Am J Pathol 1995;147:124–35.
[12] Graham MJ, Crooke ST, Monteith DK, Copper SR. Lemonidis KM, Stecker KK, Martin MJ, Crooke RM. *In vivo* distribution and metabolism of a phosphorothioate oligonucleotide within rat liver after intravenous administration. J Pharmacol Exp Ther 1998;286:447–58.
[13] Crooke RM, Graham MJ, Cooke ME, Crooke ST. *In vitro* pharmacokinetics of phosphorothioate antisense oligonucleotides. J Pharmacol Exp Ther 1995;275:462–73.
[14] Crooke ST, Graham MJ, Zuckerman JE, Brooks D, Conklin BS, Cummins LL, Grieg MJ, Guinosso CJ, Kornburst D, Maonoharan M, Sasmor HM, Schliech T, Tivel KL, Griffey RH. Pharmacokinetic properties of several novel oligonucleotides in mice. J Pharmacol Exp Ther 1996;277:923–37.
[15] Leeds JM, Graham MJ, Truong L, Cummins LL. Quantitation of phosphorothioate oligonucleotides in human plasma. Anal Biochem 1996;235:36–43.
[16] Bennett FL, Kornbrust D, Henry S, Stecker K, Howard R, Cooper S, Dutson S, Hall W, Jacoby HI. An ICAM-1 antisense oligonucleotide prevents and reverses dextran sulfate sodium-induced colitis in mice. J Pharmacol Exp Ther 1997;280:988–1000.
[17] Dean NM, McKay R. Inhibition of protein kinase C-α expression in mice after systemic administration of phosphorothioate antisense oligodeoxynucleotides. Proc Natl Acad Sci USA 1994;91:11762–6.
[18] Choi BM, Kwak HJ, Jun CD, Park SD, Kim KY, Kim HR, Chung HT. Control of scarring in adult wounds using antisense transforming growth factor-beta 1 oligodeoxynucleotide. Immunol Cell Biol 1996; 74:144–50.
[19] Monia BP, Sasmor H, Johnston JF, Freier SM, Lesnik EA, Muller M, Geiger T, Altmann K, Moser H, Fabrio D. Sequence-specific antitumor activity of a phosphorothioate oligodeoxynucelotide targeted to human C-*raf* kinase supports an antisense mechanism of action. Proc Natl Acad Sci USA 1996;93:15481–4.
[20] Iyer RP, Egan W, Regan JB, Beaucage SL. 3*H*-1,2-Benzodithiole-3-one 1,1-dioxide as an improved sulfurizing reagent in the solid-phase synthesis of oligodeoxyribonucleoside phosphorothioates. J Am Chem Soc 1990;112:1253–4.
[21] Deschenes J, Valet JP, Mareceau N. Hepatocytes from newborn and weanling rats in monolayer culture: isolation by perfusion, fibronectin-mediated adhesion, spreading and functional activities. *In Vitro* 1982;6:722–30.
[22] Seglen PO. Preparation of isolated rat liver cells. Methods Cell Biol 1976;13:29–83.
[23] Berry MN, Friend DS. High yield preparation of isolated rat liver parenchymal cells: a biochemical and fine structure analysis. J Cell Biol 1972;59:722–34.
[24] Herscowitz HB, Holden HT, Bellanti JA, Ghaffar A. Manual of macrophage methodology. New York: Marcel Dekker, 1981.
[25] Berger SL, Chirgwin JM. Isolation of RNA. Methods Enzymol 1989; 180: 3–13.
[26] Griffey RH, Greig MJ, Gaus HJ, Liu K, Monteith D, Winniman M, Cummins LL. Characterization of oligonucleotide metabolism *in vivo* via liquid chromatography/electrospray tandem mass spectrometry with a quadrupole ion trap mass spectrometer. J Mass Spectrom 1997;32:305–13.
[27] Gaus HJ, Owens SR, Winniman M, Cooper S, Cummins LL. On-line HPLC electrospray mass spectrometry of phosphorothioate oligonucleotide metabolites. Anal Chem 1997;69:313–9.
[28] Schwab G, Chavany C, Duroux I, Goubin G, Lebeau J, Helene C, Saison-Behmoaras T. Antisense oligonucleotides adsorbed to polyalkylcyanoacrylate nanoparticles specifically inhibit mutated Ha-*ras*-mediated cell proliferation and tumorgenicity in nude mice. Proc Natl Acad Sci USA 1994;91:10460–4.
[29] Yasaki T, Ahmad S, Chahlavi A, Zylber-Katz E, Dean NM, Rabkin SD, Martuza RI, Glazer RI. Treatment of glioblastoma U-87 by systemic administration of an antisense protein kinase C-α phosphorothioate oligodeoxynucleotide. Mol Pharmacol 1996;50:236–42.
[30] Perkins RA, Ward KW, Pollack GM. Comparative toxicokinetics of inhaled methanol in the female CD-1 mouse and Sprague-Dawley rat. Fundam Appl Toxicol 1995;28:245–54.
[31] Frantz SW, Beskitt JL, Grosse CM, Tallant MJ, Dietz FK, Ballantyne B. Pharmacokinetics of ethylene glycol. II. Tissue distribution, dose-dependent elimination, and identification of urinary metabolites following single intravenous, peroral or percutaneous doses in female Sprague-Dawley and CD-1 mice. Xenobiotica 1996;26:1195–220.
[32] Nomeir AA, Matthews HB. Metabolism and deposition of dimethyl hydrogen phosphite in rats and mice. J Toxicol Environ Health 1997;51:489–501.
[33] Richardson KA, Peters MM, Wong BA, Megens RH, Van Elburg PA, Booth ED, Boogaard PJ, Bond JA, Medinsky MA, Watson WP, van Sittert NJ. Quantitative and qualitative differences in the metabolism of 14C-1,3-butadiene in rats and mice: relevance to cancer susceptibility. Toxicol Sci 1999;49:186–201.
[34] Hissink AM, Oudshoorn MJ, Van Bladeren PJ. Species and strain differences in the hepatic cytochrome P450-mediated biotransformation of 1,4-dichlorobenzene. Toxicol Appl Pharmacol 1997;145:1–9.
[35] Zhuo X, Go J, Zhang QV, Spink DC, Kaminsky LS, Ding X. Biotransformation of coumarin by rodent and human cytochromes P-450: metabolic basis of tissue-selective toxicity in olfactory mucosa of rats and mice. J Pharmacol Exp Ther 1999;288:463–71.
[36] Bennett CF, Chiang M, Chan H, Shoemaker JE, Mirabelli CK. Cationic lipids enhance cellular uptake and activity of phosphorothioate antisense oligonucleotides. Mol Pharmacol 1992;41:1023–33.